



# Pansharpening Based on Low-Rank Fuzzy Fusion and Detail Supplement

Yong Yang , Senior Member, IEEE, Chenxu Wan, Shuying Huang , Member, IEEE, Hangyuan Lu, and Weiguo Wan

**Abstract**—Pansharpening is a technique used to reconstruct a high-resolution (HR) multispectral (MS) image by combining an HR panchromatic (PAN) image with a low-resolution MS image. In recent years, the detail-injection model has demonstrated excellent performance in pansharpening, thus receiving wide attention. Obtaining appropriate details is vital for the detail-injection model. Therefore, this article presents a detail optimization approach to obtain more precise high-frequency (HF) details for pansharpening. The proposed method comprises two steps. In the first step, we design a low-rank fuzzy fusion model to fuse the HF details of the PAN and MS images. In this model, the high frequencies of the PAN and upsampled MS images are decomposed into low-rank and sparse components, and the corresponding fusion rules are designed according to their characteristics. Because some details of the PAN image are replaced with those of the MS image, using them directly as injection details may result in redundant information or spatial distortion. To solve this problem and further optimize the details, in the second step, we construct an adaptive detail supplement model. Based on the similarity and correlation between the fused HF and the original HF of the PAN image, the fused details are supplemented to obtain the final injection details. Experimental results on the IKONOS, Pleiades, QuickBird, and WorldView-2 datasets demonstrate that the proposed algorithm is better than the state-of-the-art methods in maintaining spectral information and improving spatial details.

**Index Terms**—Detail-injection, detail supplementation, fuzzy logic, pansharpening.

## I. INTRODUCTION

IN RECENT years, the application of remote sensing image develops rapidly. However, the desired image with high spatial resolution and high spectral resolution cannot be obtained by the existing technology [1]–[3]. With the increasing application of high-resolution multispectral (HRMS) imaging

in environmental monitoring, spectral unmixing, water-quality evaluation, etc. [4]–[6], numerous pansharpening methods have been proposed. The method of pansharpening is to get an HRMS image by fusing high-resolution panchromatic (HRPAN) image and low-resolution multispectral (LRMS) image. At present, the traditional pansharpening methods are mainly based on [7]: component substitution (CS), multiresolution analysis (MRA), and variational optimization (VO).

The traditional CS-based method first projects a multispectral (MS) image into another spectral space; then the PAN image replaces the spatial information component of the MS image, and finally, the HRMS is obtained by reverse projection. This type of method is often referred to as the projection alternative [8]. Representative CS-based methods include intensity-hue-saturation (IHS) methods [9], [10], principal component analysis (PCA) methods [11], [12], and Gram-Schmidt methods [13]. The main advantages of these methods are simplicity with high computational efficiency and good spatial quality performance. In addition, these methods produce fewer artifacts, overlaps, and blurred textures during the fusion process. However, the disadvantage of these methods is that in the sharpened/fused images, they usually suffer from varying degrees of spectral distortion [14].

In the MRA-based method, the first step is to obtain the high- and low-frequency (LF) components of the MS images and PAN images through filter. Then, fusion on high-frequency (HF) components is performed according to some fusion rules. Finally, the HRMS is restructured by an inverse transform using the LF component of the MS image and the fused HF component. MRA-based methods include Laplace transform [15], generalized Laplacian pyramid [16], [17], à trous wavelet transform (ATWT) [18], discrete wavelet transform (DWT) [19], [20], nonsubsampling Contourlet transform [21], and nonsubsampling Shearlet transform [22]. In comparison with the CS-based methods, MRA-based methods can better retain spectral information in pansharpening images; however, they are often unsatisfactory in spatial enhancement [23].

The VO-based method is an important category of pansharpening, which includes two vital parts, the devise of the energy function and the optimization solution. The main process of this kind of pansharpening method is generally depended on, or transformed into, the optimized variational model, which includes such algorithms as P+XS [24], variational wavelet pansharpening methods [25] and sparsity-based methods [26]. These methods can obtain high precision results, but, compared

Manuscript received June 25, 2020; revised August 16, 2020; accepted September 4, 2020. Date of publication September 8, 2020; date of current version September 24, 2020. This work was supported in part by the National Natural Science Foundation of China under Grant 61662026, Grant 61862030, and Grant 62072218, and in part by the Natural Science Foundation of Jiangxi Province under Grant 20182BCB22006, Grant 20181BAB202010, Grant 20192ACB20002, and Grant 20192ACBL21008. (Corresponding author: Shuying Huang.)

Yong Yang, Chenxu Wan, and Hangyuan Lu are with the The School of Information Technology, Jiangxi University of Finance and Economics, Nanchang 330032, China (e-mail: greatyangy@126.com; wanchenxu@126.com; lhyhziee@163.com).

Shuying Huang and Weiguo Wan are with the School of Software and Internet of Things Engineering, Jiangxi University of Finance and Economics, Nanchang 330032, China (e-mail: shuyinghuang2010@126.com; wanwgplus@163.com).

Digital Object Identifier 10.1109/JSTARS.2020.3022857

with CS- or MRA-based methods, they usually have higher calculation cost and complexity [7].

With the development of deep learning in the imaging field, the pansharpening method has a new development. Masi *et al.* proposed the first pansharpening method based on convolutional neural networks in 2016, named PNN [27], and then completed other similar work within a short time [28], [29]. Recently, the pansharpening method of deep neural networks (DNNs) has been gradually developing [30]. The nonlinear DNN method can learn complex features from many samples and obtain a better fusion effect. However, these methods take a long time to train, and it is difficult to adjust network parameters optimally.

Generally, the popular and widely used CS- and MRA-based pansharpening methods aim to generate HRMS images with similar geometric resolution as in PAN images, while preserving the spectral information of MS images. To retain the overall content of LRMS images better and further increase the high spatial structure information of HRPAN images, the MRA-based injection model was developed [31]. First, the HF information of a PAN image and an MS image is obtained by filtering. Then, the obtained HF information of the PAN and MS images is fused via appropriate fusion rules. Finally, the fused HF information is injected into the MS image to obtain the final HRMS. Although some improvements have been made, there are still some problems that lead to the unsatisfactory fusion results.

- 1) The structural features of HF information are ignored. In recent years, with the development of image processing, multiscale analysis [32] has achieved great success. Remote sensing images cover a large area; thus, there are many multiscale and geometric singularities in the images. These singular points can be captured using advanced multiscale analysis tools to improve the pansharpening performance [33]. At present, most of the existing methods directly fuse the multiscale information. However, it is difficult to retain effective information pertinently without considering the structural features of multiscale information. Therefore, exploring the multiscale features of the image is helpful in improving the fusion effect. When we analyze the multiscale information of images, we find that it also exhibits low-rank features. Considering this, an effective fusion strategy that can better fuse the HF features of PAN image and MS images is required.
- 2) The HF information after fusion are not detailed enough. In the process of HF information fusion, the HF information of the PAN image is partly replaced with that of the MS image. The important information on the two images should be preserved by fusion. However, owing to the low spatial resolution of the MS images, the spatial resolution of the fused image is lower than that of the PAN image. Moreover, fused HF images may contain excessive information on the MS images. The fused HF image is not sufficiently detailed and contains redundant information from the MS image. Therefore, if the fused HF image is directly used as injection details, spatial or spectral distortion may occur in the fused image.

In this article, an optimal detail-injection method based on MRA is proposed to solve these problems. First, the HF information of PAN images and MS images is extracted through ATWT and guided filter. Then, low-rank decomposition is conducted on the extracted HF components to obtain low rank and sparse components. The low rank and sparse components are fused using fuzzy logic fusion and maximum selection rules, respectively. The fused HF component that contains the information of PAN and MS images is reconstructed by the inverse transformation. To obtain more precise HF information, an adaptive detail compensation method is proposed. The lost details can be recovered by calculating the weighting coefficient between the fused HF information and the HF information of the PAN image. Finally, the modulation coefficient is used to inject the optimized HF details into each band of the upsampled MS image to obtain the final fusion image. Compared with state-of-the-art methods, our experimental results prove that the proposed method is effective in spectral and spatial preservation.

The contributions of the proposed pansharpening method are summarized as follows.

- 1) A pansharpening method based on detail optimization is proposed. The method can effectively fuse information from MS and PAN images to enhance spatial information while maintaining spectral information.
- 2) A low-rank fuzzy fusion model is designed. According to the structural characteristics of multiscale information, a new fusion rule based on fuzzy logic is developed to fuse low-rank components. This method can effectively fuse the HF components of PAN and MS images.
- 3) A detailed supplementary scheme is presented. The scheme solves the problem of insufficient details and information redundancy in the fused image, and thus the details can be further optimized.

In the remainder of this article, we make the following arrangements. In Section II, we described the relevant work. Next, in Section III, we introduce the proposed method in detail. In Section IV, a large number of experiments and analyses are presented. Finally, in Section V, we conclude this article.

## II. RELATED WORK

In this section, we introduce the theories related to the proposed pansharpening method, including a detail-injection model based on MRA, low-rank decomposition, and fuzzy logic algorithm.

### A. Detail-Injection Scheme Based on MRA

MRA-based methods were developed in the 1980s [34]. In these methods, first, the images are decomposed into HF and LF components. Then the HF components of the PAN image and MS image are fused [35]. Finally, the fused HRMS image is obtained by inversely transforming the fused HF component and LF component of the MS image.

With the development of image fusion research, there is a new understanding of MRA-based methods. To maintain the integral content of LRMS images and further increase the spatial

structure of HRPAN images, the obtained HF spatial details are directly injected into the MS image after upsampling. The MRA-based methods can be expressed as

$$\tilde{F}_k = \tilde{M}_k + g_k (P - P_L), k = 1, 2, 3, \dots, n \quad (1)$$

where  $F_k$  and  $\tilde{M}_k$  are the  $k$ th bands of the fused HRMS image and the MS image after upsampling, respectively;  $g_k$  is the  $k$ th injection coefficient;  $n$  is the number of spatial bands of the MS image;  $P$  and  $P_L$  are the PAN image and the LF component of the PAN image, respectively.

Choi *et al.* [36] indicated that when an MS image is highly correlated with a PAN image, the HF detail information of the HRMS image is not only related to the PAN image but also related to the MS image. Therefore, the HRMS image can be defined as

$$\begin{aligned} \text{HRMS}_k &= \text{LF}(\text{HRMS}_k) + \text{HF}(\text{HRMS}_k) \\ &\approx \tilde{M}_k + g_k \text{HF}(\text{PAN}, I) \end{aligned} \quad (2)$$

where  $\text{HRMS}_k$  is the  $k$ th band of the fused HRMS image;  $\text{HF}(\text{PAN}, I)$  is the HF information concerning PAN and MS images.  $I$  represents the linear combination of MS bands and can be calculated by the following formula:

$$I = \sum_{k=1}^n \alpha_k \tilde{M}_k \quad (3)$$

where  $\alpha_k$  is the  $k$ th weighting coefficient. The specific setting of  $\alpha_k$  is detailed in [31].

An improved modulation coefficient technique is introduced in [37], which calculates the approximate relationship between the edge information of a PAN image and an MS image. In this method, the injection coefficient  $g_k$  is adaptively obtained by

$$g_k = \frac{\text{MS}_k}{\frac{1}{n} \sum_{k=1}^n \text{MS}_k} (\beta_k w_{\text{MS}_k} + (1 - \beta_k) w_P) \quad (4)$$

where  $\beta_k$  is the  $k$ th weighting parameter of MS image;  $w_{\text{MS}_k}$  and  $w_P$  are edge detection matrices representing the MS image and PAN image, respectively.

### B. Low-Rank Decomposition

A matrix can be regarded as composed of low-rank components and sparse components. A given matrix  $M$  can be decomposed into

$$M = L + S \quad (5)$$

where  $L$  denotes the low-rank component;  $S$  denotes the sparse component, and the sizes of both are arbitrary.

The column space and row space of  $L$  in low dimension are not known, nor is the dimension of  $L$ . Similarly, the position and number of nonzero elements in  $S$  are unknown. In recent years, the amount of high-dimensional data has increased dramatically in the fields of science, engineering, society, and so on. These data have a lower internal dimension. For example, they are on some low dimensional subspace [38], sparse on some basis [39], or on some low dimensional manifold [40], [41]. We can assume that these data are all located near a subspace with a

lower dimension. In other words, if all data points are stacked as a column vector of matrix  $M$ , the rank of the matrix is lower, which can be expressed mathematically as follows:

$$M = M_L + M_N \quad (6)$$

where  $M_L$  is the low-rank matrix, and  $M_N$  is the small noise matrix. The classical PCA is the best rank- $k$  estimation for solving  $M_L$  [42]

$$\begin{aligned} \min \|M - M_L\| \\ \text{s.t. } \text{rank}(M_L) \leq k \end{aligned} \quad (7)$$

where  $\|\bullet\|$  denotes the 2-norm. This problem can be solved by singular value decomposition, and it has many optimizations when noise  $M_N$  is small and identically Gaussian distributed. However, it is difficult to guarantee the validity of damaged observations. A damaged entry in  $M$  may lead to a large deviation in  $M_L$ . To solve this problem effectively, a robust PCA (RPCA) [43] was proposed, which can extract the effective  $M_L$  from the damaged observations. It can be expressed as

$$M = M_L + M_S. \quad (8)$$

The differences between (6) and (8) are that  $M_N$  is a small Gaussian noise matrix in PCA, whereas  $M_S$  is a sparse peak noise matrix of arbitrary size in RPCA. There are two ways to obtain  $M_L$  and  $M_S$ : the first method is to use the first-order method directly to solve the neighborhood problem; the second one is to transform the problem into a dual problem and determine the adjacent solution from the dual optimization solution.

### C. Fuzzy Logic

In 1965, Zadeh [44] published a pioneering article on the theory of fuzzy sets, which has attracted wide attention in the academic community. With the development of the research on fuzzy logic, the combination of fuzzy logic, neural networks, and the genetic algorithm has brought the application of fuzzy logic in many fields to reality. In recent years, researchers constantly applied the fuzzy method to the field of image fusion; for example, Yang *et al.* [45] applied type-2 fuzzy logic to medical image fusion.

Fuzzy logic is a method for describing fuzzy concepts using precise digital languages, such as fuzzy sets and membership functions. It is easy to understand, flexible, and inclusive of imprecise data. Precise sets often have “either or” relationships: they do not have the same region, but fuzzy sets are the opposite. If  $U$  is the set of object  $x$ , then the fuzzy set  $T$  of  $U$  is defined as

$$T = \{(x, \mu_T(x)) \mid x \in U\} \quad (9)$$

where  $\mu_T(x)$  is the membership function of the fuzzy set  $T$ . In other words,  $\mu_T(x)$  is the degree of membership about  $x$  of fuzzy set  $T$ , and the membership degree can change continuously with  $0 \leq \mu_T(x) \leq 1$ . The membership function has three properties: it is defined as an ordered pair; the value of the membership function is between 0 and 1; and the choice of function is subjective and personal. The membership function can be used to quantitatively describe the uncertainty between different target types and the corresponding pixels or even within each image

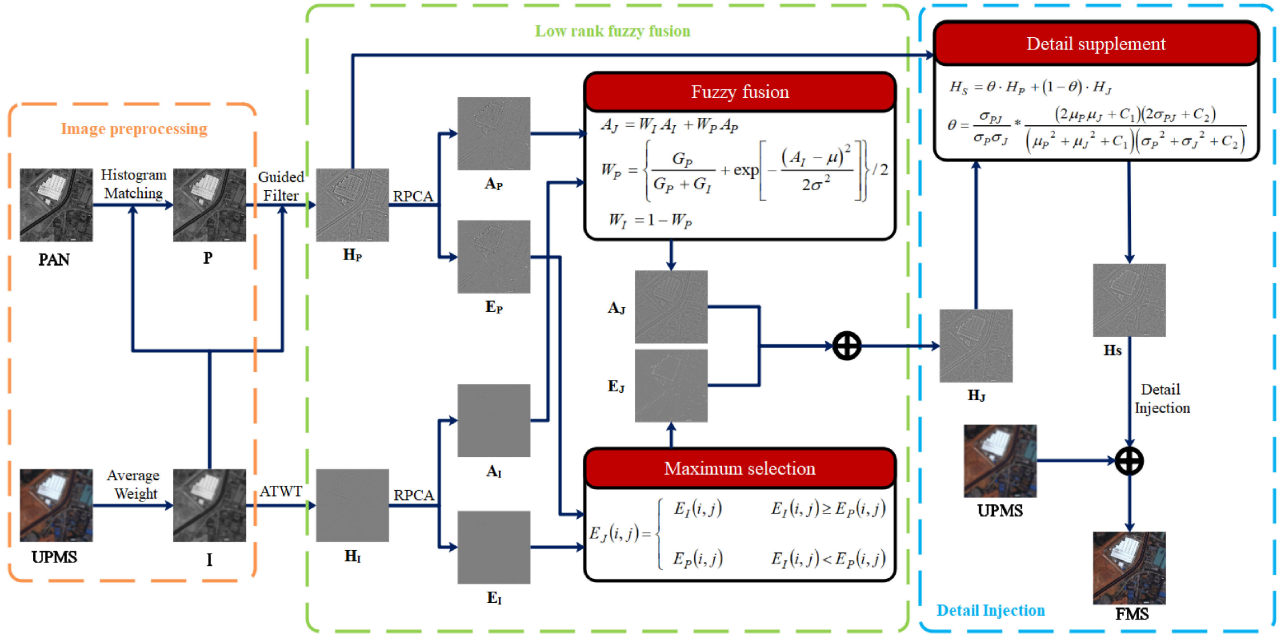


Fig. 1. Framework of the proposed method.

system. Therefore, determination of the membership function is of great significance in image fusion.

### III. PROPOSED METHOD

#### A. Overall Framework

For the traditional MRA-based methods, there is a common problem, namely, the final injected detail is not close to the ideal detail, which can result in information redundancy or spatial distortion. The best way to solve this problem is to obtain an appropriate HF detail and inject it into the upsampled MS image. Unlike existing methods, we propose two steps to obtain more ideal injection details. First, a low-rank fuzzy fusion module is designed to fuse the HF details in the PAN image and the MS image. The HF components are decomposed into low rank and sparse components. According to their different characteristics, different fusion rules are designed to obtain the fused HF components. Moreover, in the process of fusion, some information of the PAN image is replaced with information from the MS image. As a result, the resolution of the fused HF image is reduced, and the fused HF image may contain too much information from the MS image. Hence, in the second part, the details of the original PAN image are used to supplement and enhance the fused HF information to obtain the final injection HF details. Finally, we inject the obtained HF details into the up-sampled MS image to obtain the ideal fusion HRMS image. Fig. 1 illustrates the overall framework of the proposed method. The specific steps are as follows.

- 1) The MS image and PAN image are preprocessed, and the HF information  $H_I$  and  $H_P$  of  $I$  and  $P$  are extracted.
- 2) The HF information  $H_I$  and  $H_P$  are decomposed into low-rank components  $A_I$  and  $A_P$ , and sparse components  $E_I$  and  $E_P$ , respectively, by RPCA low-rank decomposition.

- 3) The fuzzy logic rule and maximum value preserving rule are designed to fuse low-rank components and sparse components, respectively. Thus, low-rank component  $A_J$  and sparse component  $E_J$  are obtained.
- 4) Low-rank component  $A_J$  and sparse component  $E_J$  are combined to obtain HF image  $H_J$ .
- 5) A detail supplement model is proposed to supplement  $H_J$  to obtain the final injection detail  $H_S$ .
- 6) The improved modulation coefficient technique is used to inject  $H_S$  into  $UPMS$  to achieve the fused image  $FMS$ .

#### B. Low-Rank Fuzzy Fusion of HF Information

Before low-rank fuzzy fusion, it is necessary to extract HF details, including MS image and PAN image information. In this article, the MS image is upsampled by bicubic interpolation to be the same size as the PAN image, and the intensity component  $I$  of the MS image is extracted. Then component  $I$  is used to match the histogram of the PAN image to obtain  $P$ . ATWT is an optimized version of DWT, which has nonorthogonality, shift-invariance, undecimated, and redundancy. It can retain the spatial information of the image more effectively. Therefore, we obtain HF information  $H_I$  from component  $I$  through ATWT. The guided filter [46] can obtain the high spatial resolution information of the input image according to the change trend of the guidance image. Hence, to reduce the impact of the difference between  $I$  and  $P$ , we adopt a guided filter with  $I$  as the guided image and  $P$  as the input image, to obtain the HF information  $H_P$ .

Most detail injection methods ignore the details of MS images, and the fused HRMS image lacks similarity to the real HRMS image. To solve this problem, this study extracted the HF information of the PAN image and the required HF information in the MS image. In the process of fusing, the HF information of



PAN and MS images, most methods ignore the fact that the HF part also contains low-rank information and sparse information. It is a rough method to fuse the HF components directly. This may cause some information that should be retained to be replaced by other unimportant information. Based on this analysis, we propose to decompose the HF components into low-rank components and sparse components for fusion. According to the characteristics of different parts, corresponding rules are designed for their fusion. The low-rank components are fused by a fuzzy logic rule, while the sparse components are selected by a maximum value strategy. This method can adaptively fuse the HF information contained in the PAN and MS images, and the fused image and the ideal image can maintain high similarity. The specific steps are as follows.

First, we decompose the HF information  $H_I$  and  $H_P$  by RPCA low-rank decomposition, and obtain the corresponding low-rank component matrices  $A_I$  and  $A_P$ , and the sparse component matrices  $E_I$  and  $E_P$

$$H_I = A_I + E_I \quad (10)$$

$$H_P = A_P + E_P. \quad (11)$$

We propose different fusion rules for low-rank components and sparse components to retain the required information. In recent years, the fuzzy logic theory has been successfully applied to image processing. Because of their peculiarity in modeling uncertainty, fuzzy-logic-based image fusion methods usually have better performance than the classical image fusion method. Thus, to express the low-rank components  $A_I$  and  $A_P$  simultaneously, a method based on fuzzy logic was designed. The fuzzy function was designed to judge the image information and make an intelligent decision on the selection of low-rank component coefficients. In this method, the effective information of two low-rank components is retained. The adaptive weighted fusion criterion is defined as follows:

$$A_J = W_I A_I + W_P A_P \quad (12)$$

where  $A_J$  is the ideal low-rank component;  $W_I$  and  $W_P$  are the weights of the corresponding low-rank components  $A_I$  and  $A_P$ , respectively, which are calculated by the following fuzzy logic function.

In fuzzy logic fusion, the choice of the membership function is especially important. We need to design the corresponding membership function according to the specific situation. In the low-rank component, the large gradient represents the rich edge information. It is not enough to only consider the edge information; we also need to consider the relationship between the local and the global image. To solve the problem of low-rank images, this study designed a new fuzzy fusion model based on gradient and Gauss function, which is called gradient and Gauss fuzzy fusion (GGFF). The gradient is used to judge the richness of the edge information, and the Gauss function is used to judge the relationship between the local and the global image. We first calculate the gradient and Gaussian membership degree of each position of  $A_I$  and  $A_P$ , and then combine them as the weight coefficients to merge the low-rank components. Denoting  $A_J$  as the fused low-rank component, then the pixels in  $A_P$  and  $A_I$

belonging to fuzzy set  $A_J$  are defined as

$$A_J = \{(x_p, \mu_P(x_p)) | x_p \in A_P\} \quad (13)$$

$$A_J = \{(x_i, \mu_I(x_i)) | x_i \in A_I\} \quad (14)$$

where  $\mu_P$  and  $\mu_I$  are the membership functions of  $A_P$  and  $A_I$ , respectively.  $x_i$  and  $x_p$  are the pixels of  $A_P$  and  $A_I$ , respectively. In the low-rank component, the gradient value represents the richness of the edge information. In order to better preserve the edge information, we design the gradient-based membership functions  $\mu_P^T$  and  $\mu_I^T$  for the  $A_P$  and  $A_I$ , respectively, which are shown as follows:

$$\mu_P^T(i, j) = \frac{G_P(i, j)}{\max(\max_{(i, j) \in P}(G_P), \max_{(i, j) \in I}(G_I))} \quad (15)$$

$$\mu_I^T(i, j) = \frac{G_I(i, j)}{\max(\max_{(i, j) \in P}(G_P), \max_{(i, j) \in I}(G_I))} \quad (16)$$

where  $G_P(i, j)$  is the gradient value of the position  $(i, j)$  in the  $A_P$ ;  $G_I(i, j)$  is the gradient value of the position  $(i, j)$  in the  $A_I$ ;  $\max(G_I)$  and  $\max(G_P)$  are the maximum gradients of  $A_I$  and  $A_P$ , respectively. The MS image contains a small amount of but valuable feature information, which is very important for the fusion result. The Gaussian function can reflect the difference between the local pixel value and the global pixel value, and the larger difference means that the local position contains more feature information. Therefore, to better retain the feature information in the MS image, we define a Gaussian function to judge whether the pixels in the MS image contain feature information. Thus, the membership function  $\mu_P^G$  and  $\mu_I^G$  of  $A_P$  and  $A_I$  based on Gaussian function are defined as

$$\mu_P^G(i, j) = \exp \left[ -\frac{(A_I(i, j) - \mu)^2}{2\sigma^2} \right] \quad (17)$$

$$\mu_I^G(i, j) = 1 - \mu_P^G(i, j) \quad (18)$$

where  $A_I(i, j)$  is the pixel value at the position  $(i, j)$  of the  $A_I$ .  $\mu$  and  $\sigma$  are the mean value and variance of low-rank component  $A_I$ . Therefore, the gradient membership functions in (15) and (16) and Gaussian membership functions in (17) and (18) are combined to design an adaptive weight coefficient as follows:

$$\begin{aligned} W_P = \mu_P &= \left( \frac{\mu_P^T}{\mu_P^T + \mu_I^T} + \mu_P^G \right) / 2 \\ &= \left\{ \frac{G_P}{G_P + G_I} + \exp \left[ -\frac{(A_I - \mu)^2}{2\sigma^2} \right] \right\} / 2. \end{aligned} \quad (19)$$

As a result, the weight coefficient of  $I$  component is defined as

$$W_I = 1 - W_P. \quad (20)$$

To verify the superiority of the proposed fuzzy membership function, we compare it with only the gradient fuzzy membership function and Gauss fuzzy membership function. The degraded data experiment was conducted on the IKONOS dataset including 60 images, and the average experimental results are shown in Table I. Bold font represents the best result, and underline represents the second best. As can be seen from the table, the combination of gradient and Gauss fuzzy membership functions

TABLE I  
AVERAGE RESULTS ON IKONOS DATASET WITH DIFFERENT  
MEMBERSHIP FUNCTIONS

	Gradient	Gauss	Gradient+Gauss
CC↑	<u>0.9423</u>	0.9420	<b>0.9424</b>
UIQI↑	<b>0.9479</b>	0.9472	<u>0.9478</u>
Q2 <sup>n</sup> ↑	<b>0.8957</b>	0.8949	<u>0.8956</u>
SAM↓	4.1085	<b>4.1051</b>	<u>4.1070</u>
ERGAS↓	<u>3.4084</u>	3.4173	<b>3.4070</b>
PSNR↑	<u>28.8697</u>	28.8588	<b>28.8813</b>

is the best for most indices, which shows that the performance of combining two membership functions is better than only one. Furthermore, in the field of image fusion, the sparse component of an image contains more feature information, which is very important. Therefore, in the sparse component fusion process, we need to keep the information contained in it to the maximum extent. Using the maximum retention principle, the information in sparse components can be effectively preserved. Therefore, the fusion rule of sparse component is defined as

$$E_J(i, j) = \begin{cases} E_I(i, j) & E_I(i, j) \geq E_P(i, j) \\ E_P(i, j) & E_I(i, j) < E_P(i, j) \end{cases} \quad (21)$$

where  $E_J$  is the fused sparse component. Finally, the low-rank component  $A_J$  and sparse component  $E_J$  are combined to obtain the HF image  $H_J$  as

$$H_J = A_J + E_J. \quad (22)$$

### C. Detail Supplement Model

In Section III-B, the fused HF information  $H_J$  is obtained. In most methods, the fused HF components of the MS and PAN image information are directly used as injection details. Although the information of the MS image is added to the fused image to ensure similarity with the ideal HRMS image, there are still some problems. In the fusion process, some information from the PAN image is replaced by information from the MS image. Therefore, if the fused HF image is taken as the injection detail directly, information redundancy and spatial resolution distortion will be caused by over supplemented MS information or insufficient PAN details. Obtaining an image that contains both PAN and MS image information and sufficient image details is a very challenging task. To solve this problem, we propose to use the HF  $H_P$  of the PAN image to supplement the details of fusion image  $H_J$ .  $H_J$  is optimized through  $H_P$  to make the final injection details more ideal. Considering the correlation and similarity between  $H_P$  and  $H_J$ , an adaptive weighting coefficient is proposed, which is used to weight the two approximate components. We consider that the correlation coefficient (CC) can measure the correlation of detail features, and the structure similarity (SSIM) [47] can measure the similarity of image structure. Thus, the weighting coefficient is defined as

$$\theta = \theta_{CC}(H_P, H_J) \theta_{SS}(H_P, H_J) \quad (23)$$

TABLE II  
AVERAGE RESULTS ON PLEIADES DATASET WITH DIFFERENT  
WEIGHTING COEFFICIENTS

	$\theta_{CC}$	$\theta_{SS}$	$\theta_{CC} * \theta_{SS}$
CC↑	0.9398	<u>0.9421</u>	<b>0.9425</b>
UIQI↑	0.9491	<u>0.9504</u>	<b>0.9506</b>
Q2 <sup>n</sup> ↑	0.8589	<u>0.8632</u>	<b>0.8640</b>
SAM↓	4.0675	<u>4.0585</u>	<b>4.0565</b>
ERGAS↓	4.5295	<u>4.4293</u>	<b>4.4094</b>
PSNR↑	27.4437	<u>27.6402</u>	<b>27.6799</b>

where  $\theta_{CC}(\bullet)$  is a function of the CC between  $H_P$  and  $H_J$ , and  $\theta_{SS}(\bullet)$  is a function of the SSIM between  $H_P$  and  $H_J$ .  $\theta_{CC}(\bullet)$  and  $\theta_{SS}(\bullet)$  can be calculated as

$$\theta_{CC}(H_P, H_J) = \frac{\sigma_{PJ}}{\sigma_P \sigma_J} \quad (24)$$

$$\theta_{SS}(H_P, H_J) = \frac{(2\mu_P \mu_J + C_1)(2\sigma_{PJ} + C_2)}{(\mu_P^2 + \mu_J^2 + C_1)(\sigma_P^2 + \sigma_J^2 + C_2)} \quad (25)$$

where  $\sigma_P$  and  $\sigma_J$  denote the standard deviation of  $H_P$  and  $H_J$ ;  $\sigma_{PJ}$  denotes the covariance of  $H_P$  and  $H_J$ ;  $\mu_P$  and  $\mu_J$  denote the mean values of  $H_P$  and  $H_J$ , respectively. Therefore, after evaluating the correlation and similarity of the  $H_P$  and  $H_J$  images, the details of image  $H_J$  are supplemented with

$$H_S = \theta \cdot H_P + (1 - \theta) \cdot H_J \quad (26)$$

where  $H_S$  denotes the final injection detail. By analyzing  $H_P$ ,  $H_J$ , and  $H_S$ , the HRMS obtained by considering  $H_S$  as the injection detail is the most similar to the ideal HRMS image. To further illustrate the effectiveness of the adaptive weight proposed in this study,  $\theta_{CC}$  and  $\theta_{SS}$  were tested separately. The degraded data experiment was conducted on the Pleiades dataset including 60 images, and the average experimental results are presented in Table II. Among all indicators, we found that the proposed combination of correlation and similarity was the best. This implies that considering similarity or correlation alone is insufficient, and combining both sides can achieve a better effect.

## IV. EXPERIMENTAL RESULTS

### A. Experimental Datasets and Comparison Methods

In this work, we apply data from four different sensor datasets: Pleiades, QuickBird, IKONOS, and WorldView-2. Each dataset includes 60 groups of source images. The sizes of the MS images and PAN images are  $256 \times 256 \times 4$  and  $1024 \times 1024$ , respectively. To fully verify the effectiveness of the proposed method, we conduct experiments on two types of databases: degraded data and real data. In the degraded data experiments, due to lack of reference image, we follow the Wald's protocol [48], and the original MS images are regarded as reference images. The low-resolution MS image is obtained by MTF [49] and nearest-neighbor sampling with a decimation factor of 4 on

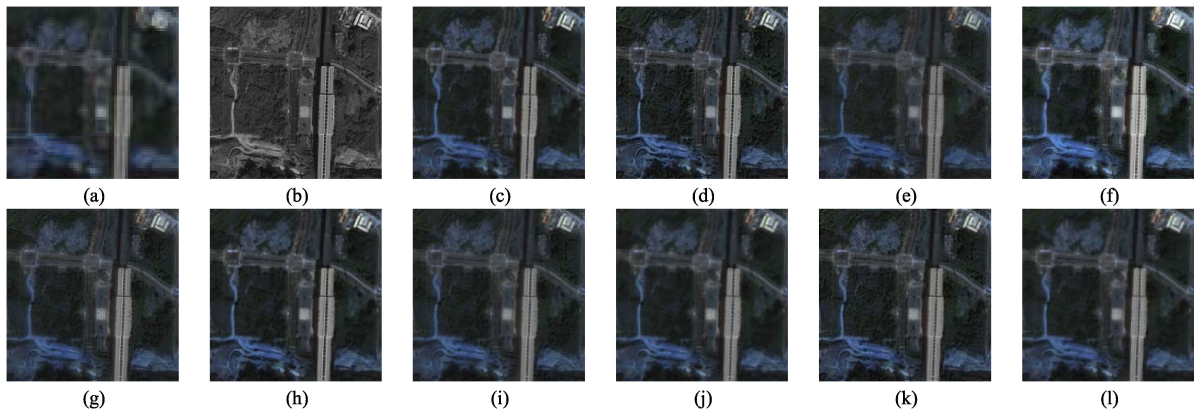


Fig. 2. Fusion results of Pleiades images. (a) MS image. (b) PAN image. (c) Reference image. (d) GSA method. (e) AIHS method. (f) BFLP method. (g) MM method. (h) IMG method. (i) MMMT method. (j) AWJDI method. (k) FSRIC method. (l) Proposed method.

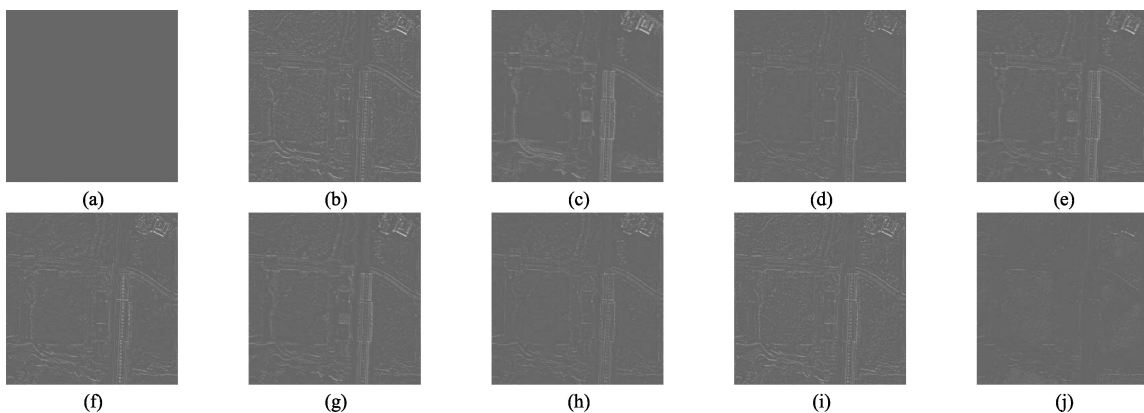


Fig. 3. Residual images estimated by the difference between the reference and pansharpened images of each algorithm in Fig. 2. (a) Ideal image. (b) GSA method. (c) AIHS method. (d) BFLP method. (e) MM method. (f) IMG method. (g) MMMT method. (h) AWJDI method. (i) FSRIC method. (j) Proposed method.

the original MS image. For the PAN image, the downsampling operation with an extraction factor of 4 is used directly.

In the test, we compared eight effective methods: the Gram Schmidt adaptive (GSA) method [50], the adaptive IHS (AIHS) method [51], the bilateral filter luminance proportional (BFLP) method [52], the matting model (MM)-based method [53], a method based on AIHS and multiscale guided filter (IMG) [37], the matting model and multiscale transform (MMMT)-based method [54], the adaptively weighted joint detail-injection method (AWJDI) [55], and the full scale regression-based injection coefficient (FSRIC) method [56]. Among them, GSA is a component substitution method and AWJDI is a method that combines variational optimization and multiresolution analysis. The remaining comparison methods are all based on multiresolution analysis. The effectiveness of our method is proved by subjective and objective comparisons. All comparison methods used in this article are public source codes provided by the corresponding authors.

### B. Quality Evaluation Indices

To illustrate the effectiveness of the proposed method quantitatively, two different sets of indicators were used for degradation data tests and real data tests, respectively. The degradation data test indicators include CC [57], universal image quality index (UIQI) [58], hypercomplex quality assessment

$Q2^n$  [59], spectral angle mapper (SAM) [60], erreur relative globale adimensionnelle de synthèse (ERGAS) [61], the root-mean-square error (RMSE) [62], and peak signal-to-noise ratio (PSNR) [63]. For real datasets, we use the quality with no reference (QNR) [64] as the evaluation index, which is composed of spectral distortion index  $D_\lambda$  and spatial distortion index  $D_S$ .

### C. Experiments on Degraded Data

In degraded data, we used datasets from Pleiades and QuickBird to evaluate the performance. Both subjective and objective experiments can show the effectiveness of the proposed method.

In the subjective comparison, only the red, green, and blue bands of the sharpened image are displayed, for the convenience of comparison. For the images from Pleiades dataset, Fig. 2(a) and (b) are degraded MS and PAN images, respectively, which are used as input images. Fig. 2(c) is the original MS image, which is used as the reference image. The fusion results are shown in Fig. 2(d)–(l). It is difficult to make a subjective comment on the resultant images directly, so the residual of the fusion results and the reference MS image is compared. Fig. 3 is the residual images, which are estimated by the difference between the reference image and the fusion result of each algorithm. Fig. 3(a) is the ideal image. Fig. 3(b)–(j) are the residual images of the fusion results of various methods. Less information on



TABLE III  
AVERAGE QUANTITATIVE RESULTS ON THE DEGRADED PLEIADES DATASET

	GSA	AIHS	BFLP	MM	IMG	MMMT	AWJDI	FSRIC	Proposed
CC $\uparrow$	0.8868	0.9259	0.9272	0.9297	0.9247	0.9259	<u>0.9396</u>	0.8908	<b>0.9425</b>
UIQI $\uparrow$	0.8944	0.9255	0.9106	0.9349	0.9376	0.9334	<u>0.9490</u>	0.8973	<b>0.9506</b>
Q2 <sup>nd</sup> $\uparrow$	0.7448	0.7903	0.7661	0.8231	0.8294	0.8129	<u>0.8588</u>	0.7521	<b>0.8640</b>
SAM $\downarrow$	8.4498	4.6870	5.7425	4.9382	4.1572	5.1023	<u>4.0687</u>	8.2785	<b>4.0566</b>
ERGAS $\downarrow$	7.4645	5.1374	7.2634	4.8814	5.2729	5.0361	<u>4.5375</u>	7.2285	<b>4.4093</b>
RMSE $\downarrow$	17.3858	12.7403	18.4446	12.3425	13.2734	12.6408	<u>11.5245</u>	16.8800	<b>11.2247</b>
PSNR $\uparrow$	23.9199	26.4091	23.5768	26.8166	26.1370	26.5570	<u>27.4272</u>	24.1863	<b>27.6800</b>

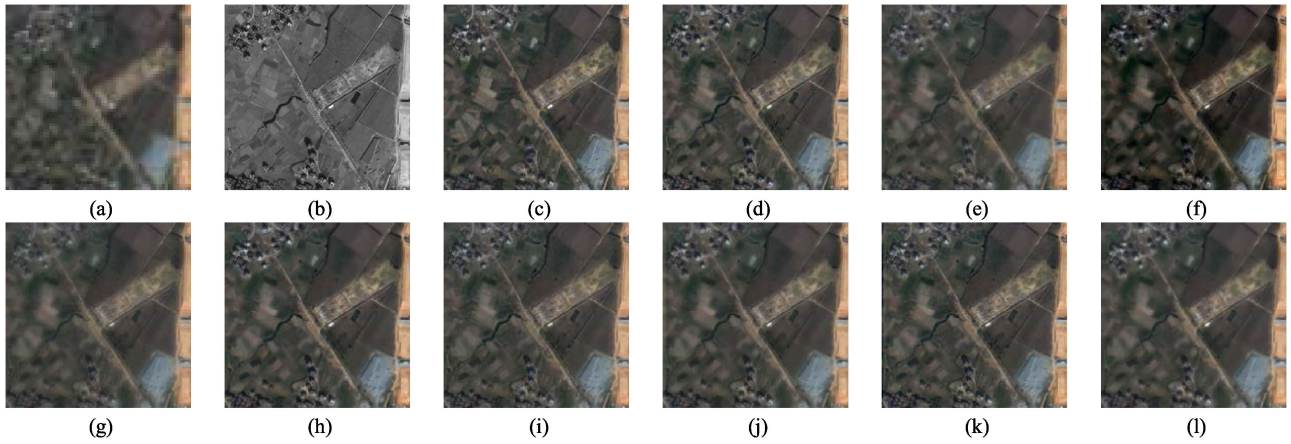


Fig. 4 Fusion results of QuickBird images. (a) MS image. (b) PAN image. (c) Reference image. (d) GSA method. (e) AIHS method. (f) BFLP method. (g) MM method. (h) IMG method. (i) MMMT method. (j) AWJDI method. (k) FSRIC method. (l) Proposed method.

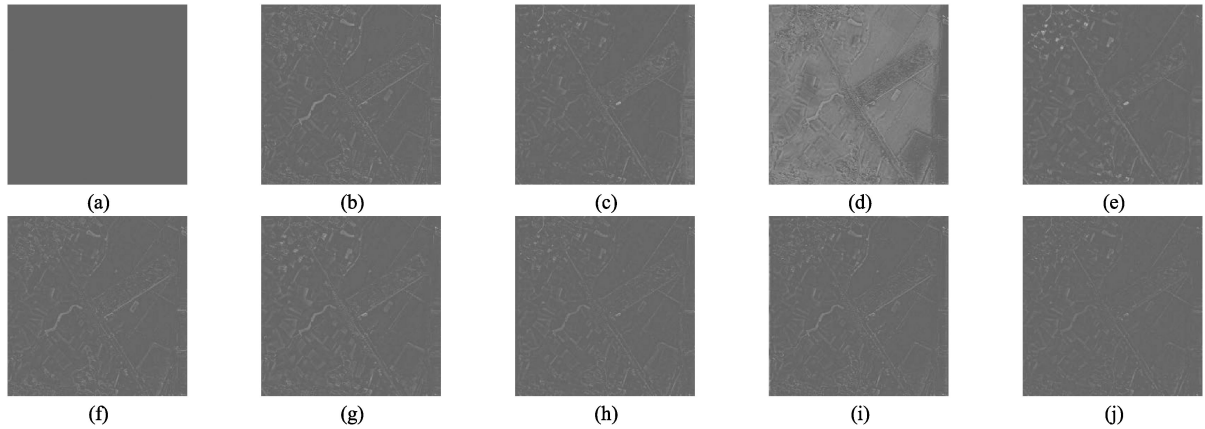


Fig. 5 Residual images estimated by the difference between the reference and pansharpened images of each algorithm in Fig. 4. (a) Ideal image. (b) GSA method. (c) AIHS method. (d) BFLP method. (e) MM method. (f) IMG method. (g) MMMT method. (h) AWJDI method. (i) FSRIC method. (j) Proposed method.

the residual image indicates a better effect of the pansharpening method. Considering both Figs. 2 and 3, the results of various pansharpening methods are analyzed. Judging subjectively, the result of the BFLP method has the problem of color deviation. The details of the GSA, MM, and FSRIC images are retained too much. By comparing the residual images, the forest area of the GSA, MM, and FSRIC images are different from the reference image. In the road area, there is a big difference between AIHS, MMMT, and the reference image. Overall, the proposed method, IMG and AWJDI have good performance.

However, the residual image of the proposed method is less than those of the other two methods. It is not difficult to see that the difference between the proposed method and the reference image is the smallest, and our method performs well in both spectral and spatial preservation. To compare the performance of all the methods better quantitatively, the average objective results of 60 images are shown in Table III. From the table, we see that the proposed method is the best in all indicators.

For the images from QuickBird dataset, Fig. 4(a) and (b) are the degraded MS and PAN images respectively, which are used



TABLE IV  
AVERAGE QUANTITATIVE RESULTS ON THE DEGRADED QUICKBIRD DATASET

	GSA	AIHS	BFLP	MM	IMG	MMMT	AWJDI	FSRIC	Proposed
CC $\uparrow$	0.8116	0.8829	0.8767	0.8787	0.8727	0.8722	<u>0.8932</u>	0.8163	<b>0.8956</b>
UIQI $\uparrow$	0.8544	0.8981	0.8795	0.9072	0.9081	0.9033	<u>0.9243</u>	0.8565	<b>0.9248</b>
Q2 $^n\uparrow$	0.7004	0.7586	0.6888	0.7796	0.7748	0.7582	<u>0.8127</u>	0.7029	<b>0.8160</b>
SAM $\downarrow$	10.9644	5.8947	6.5564	6.1157	5.6608	6.7931	<u>5.4454</u>	10.5809	<b>5.4110</b>
ERGAS $\downarrow$	8.0134	5.2286	7.8641	5.1108	5.6792	5.4032	<u>4.7272</u>	7.8417	<b>4.6389</b>
RMSE $\downarrow$	18.9632	13.0564	20.4217	12.8570	14.3974	13.4061	<u>12.0050</u>	18.5460	<b>11.8110</b>
PSNR $\uparrow$	23.7267	26.5316	22.9054	26.8071	25.7397	26.3282	<u>27.5246</u>	23.9379	<b>27.7002</b>

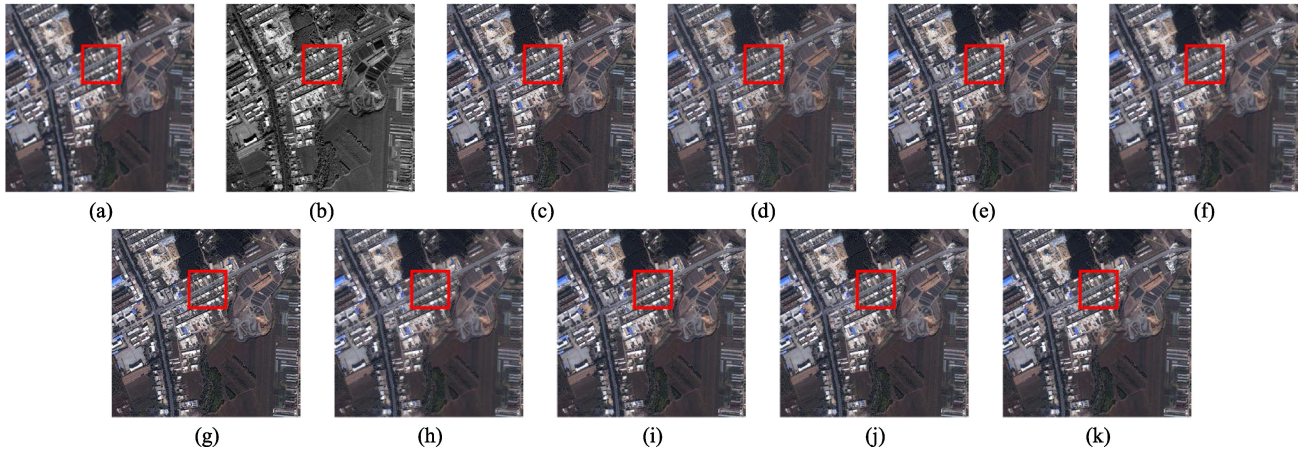


Fig. 6. Fusion results of IKONOS images. (a) MS image. (b) PAN image. (c) GSA method. (d) AIHS method. (e) BFLP method. (f) MM method. (g) IMG method. (h) MMT method. (i) AWJDI method. (j) FSRIC method. (k) Proposed method.

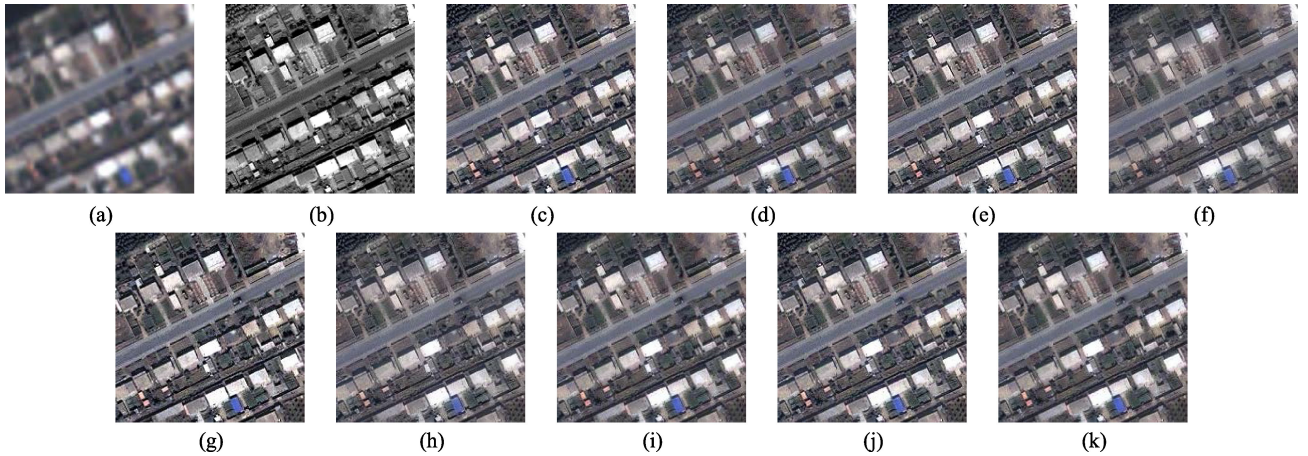


Fig. 7. Enlarged images of the marked area in Fig. 6. (a) MS image. (b) PAN image. (c) GSA method. (d) AIHS method. (e) BFLP method. (f) MM method. (g) IMG method. (h) MMT method. (i) AWJDI method. (j) FSRIC method. (k) Proposed method.

as input images. Fig. 4(c) is the original MS image, which is used as the reference image. The fusion results are shown in Fig. 4(d)–(l). Fig. 5 is the residual images, which are estimated by the difference between the reference image and the fusion result of each algorithm. Fig. 5(a) is the ideal image. Fig. 5(b)–(j) are the residual images of the fusion results of various methods. Considering Figs. 4 and 5 together, we find that BFLP is quite different from the reference image in spectrum. The result of the

MM method is too smooth, and most of the details are lost. It is difficult to make a subjective evaluation for other methods, but, from the residual images, the difference between the proposed method and the reference image is smaller than other methods. To better compare the performance of various methods, the average objective results of 60 images are shown in Table IV, where it can be seen that the proposed method is the best among all indicators.

TABLE V  
 AVERAGE QUANTITATIVE RESULTS ON THE REAL IKONOS DATASET

	GSA	AIHS	BFLP	MM	IMG	MMMT	AWJDI	FSRIC	Proposed
QNR $\uparrow$	0.6930	0.8076	0.6928	<u>0.8191</u>	0.6979	0.7863	0.8087	0.7200	<b>0.8439</b>
$D_\lambda\downarrow$	0.1855	0.1462	0.1902	<u>0.1239</u>	0.1844	0.1483	0.1378	0.1751	<b>0.1181</b>
$D_S\downarrow$	0.1502	<u>0.0542</u>	0.1474	0.0648	0.1463	0.0762	0.0620	0.1281	<b>0.0429</b>

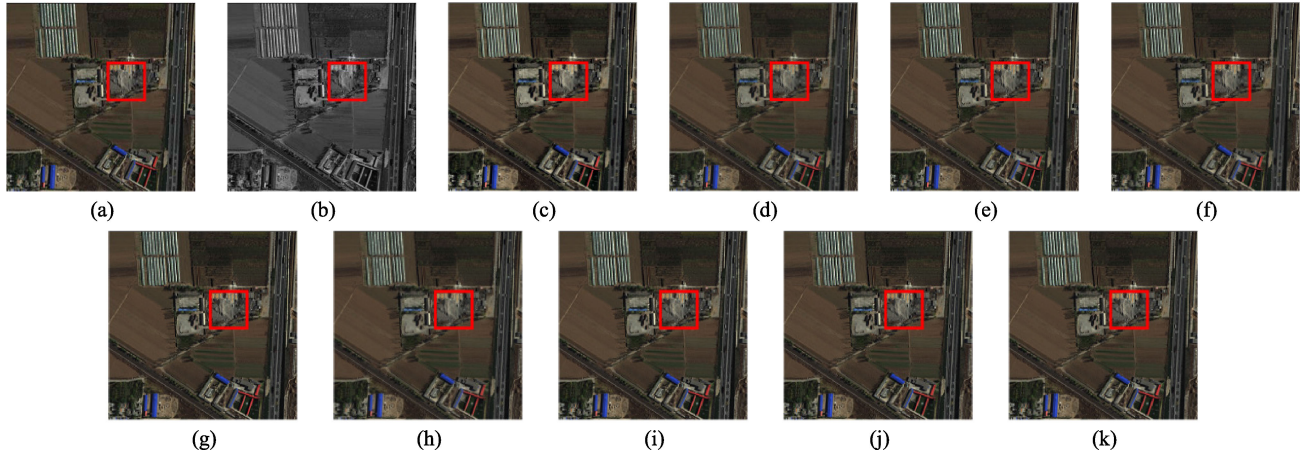


Fig. 8. Fusion results of WorldView-2 images. (a) MS image. (b) PAN image. (c) GSA method. (d) AIHS method. (e) BFLP method. (f) MM method. (g) IMG method. (h) MMT method. (i) AWJDI method. (j) FSRIC method. (k) Proposed method.

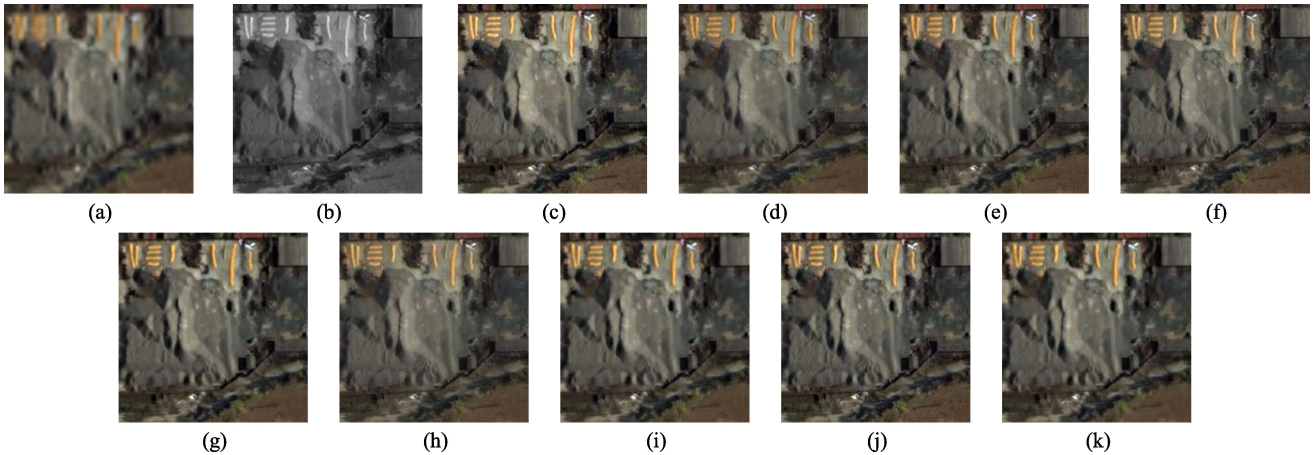


Fig. 9. Enlarged images of the marked area in Fig. 8. (a) MS image. (b) PAN image. (c) GSA method. (d) AIHS method. (e) BFLP method. (f) MM method. (g) IMG method. (h) MMT method. (i) AWJDI method. (j) FSRIC method. (k) Proposed method.

#### D. Experiments on Real Data

We conducted real data experiments on the IKONOS and WorldView-2 datasets and proved the performance of the proposed method by comparing with other methods. Because there are no reference image in the real data, we cannot give the residual image for comparison. Therefore, in the subjective evaluation, we enlarged the fusion results individually, to observe the fusion results of each method better. Both subjective and objective evaluations demonstrate the effectiveness of the proposed method.

For the images from the QuickBird dataset, Fig. 6(a) and (b) are the original MS and PAN images, respectively, which are

used as input images. The fusion results are shown in Fig. 6(c)–(k). Fig. 7(a) and (b) are the enlarged images of the red marked area for original MS and PAN images, respectively. Fig. 7(c)–(k) are the enlarged images of the red marked area for each method. From Figs. 6 and 7, we see that although the GSA, BFLP, and IMG methods perform well in details, they also introduce significant noise. The result of the MM method is too smooth, and the details are not enough. Other methods perform well in spectral and spatial preservation, but they are not as good as the proposed methods. To quantitatively compare the performance of each method, the average objective results of 60 images are shown in Table V. From the table, we can find that the proposed method achieved the best results on various indicators.



TABLE VI  
AVERAGE QUANTITATIVE RESULTS ON THE REAL WORLDVIEW-2 DATASET

	GSA	AIHS	BFLP	MM	IMG	MMMT	AWJDI	FSRIC	Proposed
QNR $\uparrow$	0.7935	0.8777	0.8397	0.8220	0.8649	0.8234	<u>0.8800</u>	0.8198	<b>0.8859</b>
$D_\lambda\downarrow$	0.0788	<b>0.0379</b>	0.0671	0.0739	0.0633	0.0712	0.0549	0.0808	<u>0.0525</u>
$D_S\downarrow$	0.1393	0.0876	0.1006	0.1128	0.0767	0.1137	<u>0.0689</u>	0.1087	<b>0.0651</b>

TABLE VII  
AVERAGE CONSUMING TIME (SECOND) OF THE COMPARISON METHODS

Methods	Degraded Data	Real Data
GSA	0.056	1.086
AIHS	0.081	0.907
BFLP	1.238	10.936
MM	0.134	2.847
IMG	0.194	2.610
MMMT	9.388	136.479
AWJDI	12.502	2942.638
FSRIC	0.061	0.798
Proposed	1.061	46.706

For the images from the WorldView-2 dataset, Fig. 8(a) and (b) are the original MS and PAN images, respectively, which are used as input images. The fusion results are depicted in Fig. 8(c)–(k). Fig. 9(a) and (b) are the enlarged images of the red marked area for original MS and PAN images, respectively. Fig. 9(c)–(k) are partially enlarged images of the red-framed area for each method. Subjective quality analysis was performed in combination with Figs. 8 and 9. Subjectively, the results of most methods are quite close, and it is difficult to evaluate whether they are good or bad. We can only comment briefly on their differences. In Fig. 9, there is a color deviation problem in the upper right corner of the MM result. In the GSA, BFLP, MM, MMT, and FSRIC results, the lower left area shows more texture, whereas in other methods, it is smoother. To better compare the performance of all the methods, the average objective results of 60 images are presented in Table VI. It can be seen from the table, the proposed method achieved the best results on most indicators.

### E. Performance Discussion

To prove the effectiveness of the low-rank fuzzy fusion model and the detail enhancement model proposed in this article, we used comparative experiments to analyze and illustrate it. The following tests were simulated on the IKONOS dataset, which contains 60 images, and evaluated by CC, UIQI, Q2n, SAM, ERGAS, RMSE, and PSNR metrics. As for the low-rank fuzzy fusion model, we compare it with two other methods. One is HF fusion with the maximum value selection rule, and the other is HF fusion with the GGFF model. The experimental results are

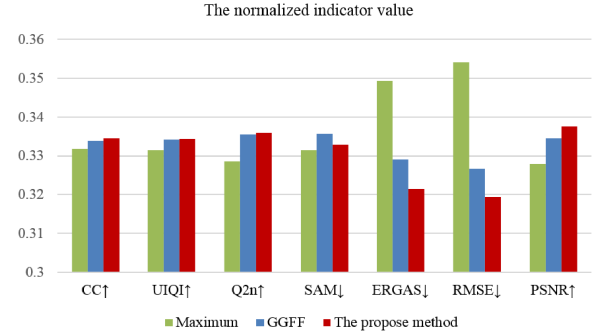


Fig. 10. Performance comparison of low-rank fuzzy fusion models.

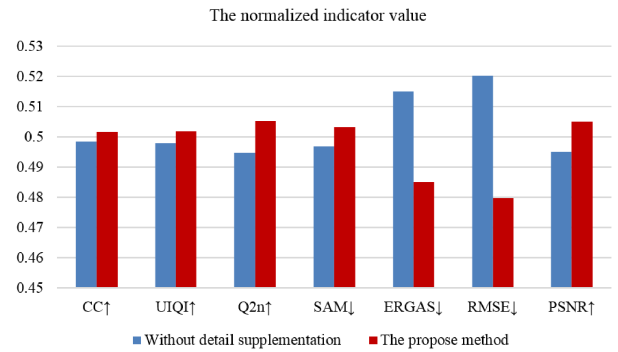


Fig. 11. Performance comparison of detail supplementation model.

shown in Fig. 10. It can be seen that the proposed method is superior to the other two methods in all indicators except SAM, which proves that the proposed low-rank fuzzy fusion algorithm is effective.

To further prove the performance of the detailed supplementation model in our method, experiments were conducted on the IKONOS dataset containing 60 images and evaluated by CC, UIQI, Q2n, SAM, ERGAS, RMSE, and PSNR metrics. We compared the results of the method with the detail supplementation model with that of the method without a detail supplementation model, and the results are shown in Fig. 11. From the figure, we see that, compared with the method without the detailed supplementation model, the proposed method with the detail supplementation model greatly improves all the indicators except SAM. The results presented here demonstrate that the detail supplementation model has a good effect.

### F. Consuming Time Comparison

To compare the computational efficiency of the proposed method and the comparison methods, the average running time



of the fusion methods is presented. Table VII summarizes the average running time consumed by experiments on both degraded data and real data. The degraded dataset and the real dataset each contain 120 images. The time consumption of GSA, AIHS, and FSRIC is extremely low, followed by MM and IMG. The time consumption of the BFLP method in the degradation data test is larger than that of the proposed method; however, it is smaller than ours in the real data test. The time consumed by MMT and AWJDI is much larger than that by the proposed method. Therefore, based on all the above-mentioned experimental results and the running time comparison here, it can be inferred that the proposed method improves the performance of fusion with acceptable consuming time.

## V. DISCUSSION

In the detail injection-based pansharpening method, in order to make the result closer to the real result, the injected details need to contain enough information on MS and PAN images. Most methods get the injected details by fusing HF components of MS and PAN images, which is a rough fusion method. To obtain more reliable details, this article proposes two models to obtain injected details closer to the real HR MS image.

First, to better fuse the details of PAN and MS images, we propose a fusion method based on low-rank decomposition and fuzzy fusion to obtain the preliminary fused HF component. In the work, the HF components of MS and PAN images are decomposed into low-rank and sparse components, and then the corresponding rules are set according to the properties of different components. The low-rank component mainly contains the approximate features of the image, reflecting the contour information of the image, and occupying the main energy of the image. The common low-rank component fusion criteria include weighted average method, max-local-energy method, and max-local-variance method. However, the weighted average method does not consider the edge and brightness characteristics of the image, which reduces the contrast of the fused image and affects the visual effect of the fused image. The max-local-energy method tends to select high-brightness areas, which refines the edges of low-brightness areas. The max-local-variance method gives priority to the areas with rich edge texture, which ignores the influence of brightness, and is more sensitive to noise. Since fuzzy logic is good at expressing qualitative knowledge and experience with unclear boundaries, this article applies fuzzy logic algorithms to image fusion based on the characteristics of the low-rank component, so as to better retain the useful information from the low-rank component. The sparse component contains important details such as the edges, lines, and boundaries of the image. In this article, the absolute maximum rule is adopted for sparse components. The algorithm is simple, saves computing time and improves image processing speed, while retaining the details to the maximum extent. Then, the fused low-rank and sparse components are combined to obtain the preliminary HF component.

Furthermore, in the fusion process, some information from the PAN image is replaced by the information from the MS image. Therefore, if the fused HF component is directly used

as the injection details, the information redundancy and spatial resolution distortion will be caused by excessively supplemented MS information or insufficient PAN details. In order to further improve the fused image, we then designed a detail supplement model, which can supplement the details of the preliminary HF component by calculating the correlation and similarity between the HF component of the PAN image and the fused HF component to obtain the final injected details. Finally, the improved modulation coefficient technique is employed to inject the obtained details into the up-sampled MS image to achieve the final fused image. Experimental results show that the proposed method has the best performance on both degraded data and real data.

Since the low-rank decomposition and fuzzy fusion strategy has a certain computational complexity, the proposed method takes a longer time than some traditional method, but it takes less time than the variational optimization-based methods, like sparse representation. In the work, we conducted experiments on four datasets. Although we did not include all scenarios, it still shows that our method is generalizable to a certain extent. However, due to the spatial details of the introduced information from MS image are relatively fuzzy, the final fused image of most methods is difficult to achieve the desired effect. How to introduce MS information without reducing the spatial quality of the fusion image is still worth studying. In addition, like most of the literature, this article conducts experiments on remote sensing images with good registration and quality, so some other important progresses in image fusion are ignored. Actually, for remote sensing image fusion, in addition to spectral and spatial inconsistency, we also need to pay attention to the haze effect of images, the misaligned MS and PAN images, and the effects of point spread function. For example, Li *et al.* [65] proposed a PAN-modulation-based pansharpening method taking account of haze, which is referred as a Haze- and Ratio-based method. For images with registration problems, Jing *et al.* [66] proposed an image fusion method for misaligned panchromatic and MS data. Spatial downscaling is an ill-posed inverse problem, Wang *et al.* [67] proposed a multiresolution image fusion guided by information loss. Pardo-Iguzquiza *et al.* proposed a downscaling co-kriging method for image sharpening [68], which can explicitly take into account the point spread function of the sensor and has the property of prediction coherence. In the future work, we will consider the above factors in pansharpening.

## VI. CONCLUSION

This article presents a pansharpening method based on detail optimization to obtain a more reliable injection detail. Unlike the traditional method of obtaining details, first, the HF details of MS images and PAN images are fused by the proposed low-rank fuzzy fusion method. Next, we constructed the detail supplement model to supplement the fused details to obtain the final injection details. Finally, the modulation coefficient was used to inject the details into each band of the MS image to obtain the final fusion HRMS image. The Pleiades, QuickBird, IKONOS, and WorldView-2 datasets were used to verify the performance of the proposed method. Through the degradation data and real data

experiments, and comparison with a series of state-of-the-art methods, the experimental results demonstrate that the proposed method can improve the detail information while maintaining spectral information. In the future, we intend to further study the structural characteristics of multiscale information and further improve the detail information while maintaining the spectral information.

## REFERENCES

- [1] H. K. Zhang and B. Huang, "A new look at image fusion methods from a bayesian perspective," *Remote Sens.*, vol. 7, no. 6, pp. 6828–6861, 2015.
- [2] B. Aiuzzi, L. Alparone, S. Baronti, R. Carlà, A. Garzelli, and L. Santurri, "Sensitivity of pansharpening methods to temporal and instrumental changes between multispectral and panchromatic data sets," *IEEE Trans. Geosci. Remote Sens.*, vol. 55, no. 1, pp. 308–319, Jan. 2017.
- [3] L. Hou and X. Zhang, "Pansharpening image fusion using cross-channel correlation: A framelet-based approach," *J. Math. Imaging Vis.*, vol. 55, no. 1, pp. 36–49, 2016.
- [4] G. Simone, A. Farina, F. C. Morabito, S. B. Serpico, and L. Bruzzone, "Image fusion techniques for remote sensing applications," *Inf. Fusion*, vol. 3, no. 1, pp. 3–15, 2002.
- [5] N. Chang, K. Bai, S. Imen, C. Chen, and W. Gao, "Multisensor satellite image fusion and networking for all-weather environmental monitoring," *IEEE Syst. J.*, vol. 12, no. 2, pp. 1341–1357, Jun. 2018.
- [6] Q. Wei, N. Dobigeon, and J. Tourneret, "Bayesian fusion of multi-band images," *IEEE J. Sel. Top. Signal Process.*, vol. 9, no. 6, pp. 1117–1127, Sep. 2015.
- [7] X. Meng, H. Shen, H. Li, L. Zhang, and R. Fu, "Review of the pansharpening methods for remote sensing images based on the idea of meta-analysis: Practical discussion and challenges," *Inf. Fusion*, vol. 46, pp. 102–113, 2019.
- [8] C. Thomas, T. Ranchin, L. Wald, and J. Chanussot, "Synthesis of multispectral images to high spatial resolution: A critical review of fusion methods based on remote sensing physics," *IEEE Trans. Geosci. Remote Sens.*, vol. 46, no. 5, pp. 1301–1312, May 2008.
- [9] W. Carper, T. Lillesand, and R. Kiefer, "The use of intensity-hue-saturation transformations for merging spot panchromatic and multispectral image data," *Photogramm. Eng. Remote Sens.*, vol. 56, no. 4, pp. 459–467, 1990.
- [10] J. A. Malpica, "Hue adjustment to IHS pan-sharpened IKONOS imagery for vegetation enhancement," *IEEE Geosci. Remote Sens. Lett.*, vol. 4, no. 1, pp. 27–31, Jan. 2007.
- [11] Z. Wang, D. Ziou, C. Armenakis, D. Li, and Q. Li, "A comparative analysis of image fusion methods," *IEEE Trans. Geosci. Remote Sens.*, vol. 43, no. 6, pp. 1391–1402, Jun. 2005.
- [12] V. K. Shettigara, "A generalized component substitution technique for spatial enhancement of multispectral images using a higher resolution data set," *Photogramm. Eng. Remote Sens.*, vol. 58, no. 5, pp. 561–567, 1992.
- [13] C. A. Laben and B. V. Brower, "Process for enhancing the spatial resolution of multispectral imagery using pan-sharpening," U.S. Patent 6 011 875, Jan. 2000.
- [14] C. Chen, Y. Li, W. Liu, and J. Huang, "SIRF: Simultaneous satellite image registration and fusion in a unified framework," *IEEE Trans. Image Process.*, vol. 24, no. 11, pp. 4213–4224, Nov. 2015.
- [15] B. Aiuzzi, L. Alparone, S. Baronti, A. Garzelli, and M. Selva, "MTF-tailored multiscale fusion of high-resolution MS and Pan imagery," *Photogramm. Eng. Remote Sens.*, vol. 72, no. 5, pp. 591–596, 2006.
- [16] L. Alparone, B. Aiuzzi, S. Baronti, and A. Garzelli, "Sharpening of very high resolution images with spectral distortion minimization," in *Proc. IEEE Int. Geosci. Remote Sensing Symp.*, 2003, vol. 1, pp. 458–460.
- [17] B. Aiuzzi, L. Alparone, S. Baronti, and A. Garzelli, "Context-driven fusion of high spatial and spectral resolution images based on oversampled multiresolution analysis," *IEEE Trans. Geosci. Remote Sens.*, vol. 40, no. 10, pp. 2300–2312, Oct. 2002.
- [18] J. Nunez, X. Otazu, O. Fors, A. Prades, V. Pala, and R. Arbiol, "Multiresolution-based image fusion with additive wavelet decomposition," *IEEE Trans. Geosci. Remote Sensing*, vol. 37, no. 3, pp. 1204–1211, May 1999.
- [19] B. Garguet-Dupont, J. Girel, J.-M. Chassery, and G. Patou, "The use of multiresolution analysis and wavelets transform for merging SPOT panchromatic and multispectral image data," *Photogramm. Eng. Remote Sens.*, vol. 62, no. 9, pp. 1057–1066, 1996.
- [20] S. Li, J. T. Kwok, and Y. Wang, "Using the discrete wavelet frame transform to merge Landsat TM and SPOT panchromatic images," *Inf. Fusion*, vol. 3, no. 1, pp. 17–23, 2002.
- [21] A. L. Da Cunha, J. Zhou, and M. N. Do, "The Nonsampled contourlet transform: Theory, design, and applications," *IEEE Trans. Image Process.*, vol. 15, no. 10, pp. 3089–3101, Oct. 2006.
- [22] M. Yin, W. Liu, X. Zhao, Y. Yin, and Y. Guo, "A novel image fusion algorithm based on nonsampled shearlet transform," *Optik*, vol. 125, no. 10, pp. 2274–2282, 2014.
- [23] H. Ghassemian, "A review of remote sensing image fusion methods," *Inf. Fusion*, vol. 32, no. PA, pp. 75–89, 2016.
- [24] C. Ballester, V. Caselles, L. Igual, J. Verdera, and B. Rougé, "A variational approach for P+ XS image fusion," *Int. J. Comput. Vis.*, vol. 69, no. 1, pp. 43–58, 2006.
- [25] M. Möller, T. Wittman, A. L. Bertozzi, and M. Burger, "A variational approach for sharpening high dimensional images," *SIAM J. Imaging Sci.*, vol. 5, no. 1, pp. 150–178, 2012.
- [26] X. X. Zhu and R. Bamler, "A sparse image fusion algorithm with application to pan-sharpening," *IEEE Trans. Geosci. Remote Sens.*, vol. 51, no. 5, pp. 2827–2836, May 2013.
- [27] G. Masi, D. Cozzolino, V. Erdoliva, and L. G. Scarpa, "Pansharpening by convolutional neural networks," *Remote Sens.*, vol. 8, no. 7, 2016, Art. no. 594.
- [28] Y. Wei, Q. Yuan, H. Shen, and L. Zhang, "Boosting the accuracy of multispectral image pansharpening by learning a deep residual network," *IEEE Geosci. Remote Sens. Lett.*, vol. 14, no. 10, pp. 1795–1799, Oct. 2017.
- [29] Q. Yuan, Y. Wei, X. Meng, H. Shen, and L. Zhang, "A multiscale and multidepth convolutional neural network for remote sensing imagery pansharpening," *IEEE J. Sel. Top. Appl. Earth Observ. Remote Sens.*, vol. 11, no. 3, pp. 978–989, Mar. 2018.
- [30] H. Shen, X. Meng, and L. Zhang, "An Integrated framework for the spatio-temporal-spectral fusion of remote sensing images," *IEEE Trans. Geosci. Remote Sens.*, vol. 54, no. 12, pp. 7135–7148, Dec. 2016.
- [31] G. Vivone *et al.*, "A critical comparison among pansharpening algorithms," *IEEE Trans. Geosci. Remote Sens.*, vol. 53, no. 5, pp. 2565–2586, May 2015.
- [32] W. Dong, S. Xiao, X. Xue, and J. Qu, "An improved hyperspectral pansharpening algorithm based on optimized injection model," *IEEE Access*, vol. 7, pp. 16718–16729, 2019.
- [33] H. Li, W. Li, G. Han, and F. Liu, "Coupled tensor decomposition for hyperspectral pansharpening," *IEEE Access*, vol. 6, pp. 34206–34213, 2018.
- [34] R. A. Schowengerdt, "Reconstruction of multispatial, multispectral image data using spatial frequency content," *Photogramm. Eng. Remote Sens.*, vol. 46, no. 10, pp. 1325–1334, 1980.
- [35] B. Aiuzzi, S. Baronti, F. Lotti, and M. Selva, "A comparison between global and context-adaptive pansharpening of multispectral images," *IEEE Geosci. Remote Sens. Lett.*, vol. 6, no. 2, pp. 302–306, Apr. 2009.
- [36] J. Choi, K. Yu, and Y. Kim, "A new adaptive component-substitution-based satellite image fusion by using partial replacement," *IEEE Trans. Geosci. Remote Sens.*, vol. 49, no. 1, pp. 295–309, Jan. 2011.
- [37] Y. Yang, W. Wan, S. Huang, F. Yuan, S. Yang, and Y. Que, "Remote sensing image fusion based on adaptive IHS and multiscale guided filter," *IEEE Access*, vol. 4, pp. 4573–4582, 2016.
- [38] C. Eckart and G. Young, "The approximation of one matrix by another of lower rank," *Psychometrika*, vol. 1, no. 3, pp. 211–218, 1936.
- [39] S. S. Chen, D. L. Donoho, and M. A. Saunders, "Atomic decomposition by basis pursuit," *SIAM Rev.*, vol. 43, no. 1, pp. 129–159, 2001.
- [40] J. B. Tenenbaum, V. De Silva, and J. C. Langford, "A global geometric framework for nonlinear dimensionality reduction," *Science*, vol. 290, no. 5500, pp. 2319–2323, 2000.
- [41] M. Belkin and P. Niyogi, "Laplacian eigenmaps for dimensionality reduction and data representation," *Neural Comput.*, vol. 15, no. 6, pp. 1373–1396, 2003.
- [42] J. Yu, "Rank-constrained PCA for intrinsic images decomposition," in *Proc. IEEE Int. Conf. Image Process.*, 2016, pp. 3578–3582.
- [43] B. E. Moore, R. R. Nadakuditi, and J. A. Fessler, "Improved Robust PCA using low-rank denoising with optimal singular value shrinkage," in *Proc. IEEE Workshop Statist. Signal Process.*, 2014, pp. 13–16.
- [44] L. A. Zadeh, "Fuzzy sets," *Inf. Control*, vol. 8, no. 3, pp. 338–353, 1965.
- [45] Y. Yang, Y. Que, S. Huang, and P. Lin, "Multimodal sensor medical image fusion based on type-2 fuzzy logic in NSCT domain," *IEEE Sens. J.*, vol. 16, no. 10, pp. 3735–3745, May 2016.
- [46] K. He, J. Sun, and X. Tang, "Guided image filtering," *IEEE Trans. Pattern Anal. Mach. Intell.*, vol. 35, no. 6, pp. 1397–1409, Jun. 2013.

- [47] Z. Wang, A. C. Bovik, H. R. Sheikh, and E. P. Simoncelli, "Image quality assessment: from error visibility to structural similarity," *IEEE Trans. Image Process.*, vol. 13, no. 4, pp. 600–612, Apr. 2004.
- [48] L. Wald, T. Ranchin, and M. Mangolini, "Fusion of satellite images of different spatial resolutions: Assessing the quality of resulting images," *Photogramm. Eng. Remote Sens.*, vol. 63, no. 6, pp. 691–699, 1997.
- [49] B. Aiazzi, L. Alparone, S. Baronti, A. Garzelli, and M. Selva, "MTF-tailored multiscale fusion of high-resolution MS and panimagery," *Photogramm. Eng. Remote Sens.*, vol. 72, pp. 591–596, May 2006.
- [50] B. Aiazzi, S. Baronti, and M. Selva, "Improving component substitution pansharpening through multivariate regression of MS+Pan Data," *IEEE Trans. Geosci. Remote Sensing*, vol. 45, no. 10, pp. 3230–3239, Oct. 2007.
- [51] S. Rahmani, M. Strait, D. Merkurjev, M. Moeller, and T. Wittman, "An adaptive IHS pan-sharpening method," *IEEE Geosci. Remote Sens. Lett.*, vol. 7, no. 4, pp. 746–750, Oct. 2010.
- [52] N. H. Kaplan and I. Erer, "Bilateral filtering-based enhanced pansharpening of multispectral satellite images," *IEEE Geosci. Remote Sens. Lett.*, vol. 11, no. 11, pp. 1941–1945, Nov. 2014.
- [53] X. Kang, S. Li, and J. A. Benediktsson, "Pansharpening with matting model," *IEEE Trans. Geosci. Remote Sens.*, vol. 52, no. 8, pp. 5088–5099, Aug. 2014.
- [54] Y. Yang, W. Wan, S. Huang, P. Lin, and Y. Que, "A novel pan-sharpening framework based on matting model and multiscale transform," *Remote Sens.*, vol. 9, no. 4, p. 391, 2017.
- [55] Y. Yang, L. Wu, S. Huang, W. Wan, and Y. Que, "Remote sensing image fusion based on adaptively weighted joint detail injection," *IEEE Access*, vol. 6, pp. 6849–6864, 2018.
- [56] G. Vivone, R. Restaino, and J. Chanussot, "Full scale regression-based injection coefficients for panchromatic sharpening," *IEEE Trans. Image Process.*, vol. 27, no. 7, pp. 3418–3431, Jul. 2018.
- [57] X. X. Zhu and R. Bamler, "A sparse image fusion algorithm with application to pan-sharpening," *IEEE Trans. Geosci. Remote Sens.*, vol. 51, no. 5, pp. 2827–2836, May 2013.
- [58] Z. Wang and A. C. Bovik, "A universal image quality index," *IEEE Signal Process. Lett.*, vol. 9, no. 3, pp. 81–84, Mar. 2002.
- [59] A. Garzelli and F. Nencini, "Hypercomplex quality assessment of multi/hyperspectral images," *IEEE Geosci. Remote Sens. Lett.*, vol. 6, no. 4, pp. 662–665, Oct. 2009.
- [60] L. Alparone, L. Wald, J. Chanussot, C. Thomas, P. Gamba, and L. M. Bruce, "Comparison of pansharpening algorithms: Outcome of the 2006 GRS-S data-fusion contest," *IEEE Trans. Geosci. Remote Sens.*, vol. 45, no. 10, pp. 3012–3021, Oct. 2007.
- [61] L. Wald, "Quality of high resolution synthesised images: Is there a simple criterion?" in *Proc. Int. Conf. Fusion Earth Data*, Jan. 2000, pp. 99–103.
- [62] Y. Yang, S. Tong, S. Huang, and P. Lin, "Multifocus image fusion based on NSCT and focused area detection," *IEEE Sensors J.*, vol. 15, no. 5, pp. 2824–2838, May 2015.
- [63] Z. H. Nezhad, A. Karami, R. Heylen, and P. Scheunders, "Fusion of Hyperspectral and multispectral images using spectral unmixing and sparse coding," *IEEE J. Sel. Top. Appl. Earth Observ. Remote Sens.*, vol. 9, no. 6, pp. 2377–2389, Jun. 2016.
- [64] L. Alparone, B. Aiazzi, S. Baronti, A. Garzelli, F. Nencini, and M. Selva, "Multispectral and panchromatic data fusion assessment without reference," *Photogramm. Eng. Remote Sens.*, vol. 74, no. 2, pp. 193–200, 2008.
- [65] H. Li and L. Jing, "Improvement of a pansharpening method taking into account haze," *IEEE J. Sel. Top. Appl. Earth Observ. Remote Sens.*, vol. 10, no. 11, pp. 5039–5055, Nov. 2017.
- [66] L. Jing and Q. Cheng, "An image fusion method for misaligned panchromatic and multispectral data," *Int. J. Remote Sens.*, vol. 32, no. 4, pp. 1125–1137, 2011.
- [67] Q. Wang, W. Shi, and P. M. Atkinson, "Information loss-guided multi-resolution image fusion," *IEEE Trans. Geosci. Remote Sens.*, vol. 58, no. 1, pp. 45–57, Jan. 2020.
- [68] E. Pardo-Igúzquiza, M. Chica-Olmo, and P. M. Atkinson, "Downscaling cokriging for image sharpening," *Remote Sens. Environ.*, vol. 102, no. 1–2, pp. 86–98, 2006.



Prof. Yang is an Associate Editor of the *IEEE ACCESS* and an Editor of the *KSII Transactions on Internet and Information Systems*.



**Chenxu Wan** received the B.S. degree in software engineering from Jiangxi Normal University, Nanchang, China, in 2018. He is currently pursuing the M.S. degree in computer science and technology at Jiangxi University of Finance and Economics, Nanchang, China.

His current research interests include image fusion, fuzzy logic, and sparse representation.



**Shuying Huang** (Member, IEEE) received the Ph.D. degree in computer application technology from Ocean University of China, Qingdao, China, in 2013.

She is currently an Associate Professor with the School of Software and Internet of Things Engineering, Jiangxi University of Finance and Economics, Nanchang, China. Her current research interests include image and signal processing, and pattern recognition.



**Hangyuan Lu** received the B.S. degree and M.S. degree in detection technology and automation device from Hangzhou Dianzi University, Zhejiang, China, in 2009. He is currently pursuing the Ph.D. degree in computer technology at Jiangxi University of Finance and Economics, Nanchang.

His current research interests include image fusion, sparse representation, and deep learning.



**Weiguo Wan** received the B.S. degree in mathematics and applied mathematics from Jiangxi Normal University, Nanchang, China, in 2014 and Ph.D. degree in computer science and engineering from Jeonbuk National University, Jeonju, South Korea, in 2020.

He is currently a Lecturer with the School of Software and Internet of Things Engineering, Jiangxi University of Finance and Economics, Nanchang, China. His current research interests include computer vision, deep learning, face sketch synthesis and recognition, and remote sensing image fusion.